A combined remote sensing–numerical modelling approach to the stability analysis of Delabole Slate Quarry, Cornwall, UK

Mohsen Havaej [a], John Coggan [b], Doug Stead [a], Davide Elmo [c]

[a] Simon Fraser University, Burnaby, British Columbia, Canada

[b] Camborne School of Mines, University of Exeter, Cornwall, UK

[c] University of British Columbia, Vancouver, British Columbia, Canada

1. Abstract

Rock slope geometry and discontinuity properties are among the most important factors in realistic rock slope analysis yet they are often oversimplified in numerical simulations. This is primarily due to the difficulties in obtaining accurate structural and geometrical data as well as the stochastic representation of discontinuities. Recent improvements in both digital data acquisition and incorporation of discrete fracture network data into numerical modelling software have provided better tools to capture rock mass characteristics, slope geometries and digital terrain models allowing more effective modelling of rock slopes. Advantages of using improved data acquisition technology include safer and faster data collection, greater areal coverage, and accurate data geo-referencing far exceed limitations due to orientation bias and occlusion. A key benefit of a detailed point cloud dataset is the ability to measure and evaluate discontinuity characteristics such as orientation, spacing/intensity and persistence. This data can be used to develop a discrete fracture network (DFN) which can be imported into the numerical simulations to study the influence of the stochastic nature of the discontinuities on the failure mechanism. We demonstrate the application of digital terrestrial photogrammetry in discontinuity characterization and distinct element simulations within a slate quarry. An accurately georeferenced photogrammetry model is used to derive the slope geometry and to characterize geological structures. We first show how a discontinuity dataset, obtained from a photogrammetry model can be used to characterize discontinuities and to develop discrete fracture networks. A deterministic three dimensional distinct element model is then used to investigate the effect of some key input parameters (friction angle, spacing and persistence) on the stability of the quarry slope model. Finally, adopting a stochastic approach, discrete fracture networks are used as input for 3D distinct element simulations to better understand the stochastic nature of the geological structure and its effect on the quarry slope failure mechanism. The numerical modelling results highlight the influence of discontinuity characteristics and kinematics on the slope failure mechanism and the variability in the size and shape of the failed blocks.

2. Introduction

High quality slate has been quarried at Delabole Slate Quarry, located in Cornwall, United Kingdom (Figure 1) for several centuries (Coggan and Pine 1996). The Delabole Slates are fine-grained, greenish grey quartz-chlorite-sericite slates with small, oval-shaped pyrite spots that are interbedded with limestone parting and coarser arenaceous beds (Freshney 1972). The Delabole Slates lay within the Tintagel Succession; specifically the Delabole Member within the Tredorn Slate Formation (Selwood et al. 1998). The Delabole Member is a lenticular body which has an arcuate outcrop shape around the Davidstow anticline. Three phase of deformation (D_{1-3}) have been recognised. The first is a ductile folding episode followed by thrusting and shear folding, overprinted by extensional features (Selwood et al. 1998). The South West region of the United Kingdom lies on the northern fringes of the Variscan Orogen, a mountain building episode which occurred during the Devonian and early Carboniferous. Consequently, the stratigraphy of the region was divided by a series of complex folds and thrusts and the intrusions of several granite plutons.

The stratigraphy of North Cornwall was controlled by extensional half-grabens, in which thick basinal sequences accumulated during the Devonian and Carboniferous. The area around the Delabole Quarry was positioned on the southern edge of the continental mass of Laurasia, a region known as Eastern Aralonia. Sedimentation occurred on the edge of the continental crust in response to intra-shelf basin development. According to Selwood et al. (1998) later faulting, that cuts across all the Variscan features, are also observed within the area. The metamorphic history of North Cornwall (the Tintagel High Strain Zone) is influenced by anchizone and epizone metamorphisms and contact or thermal metamorphisms due to the intrusion of the Bodmin Moor granite to the south east (Selwood et al., 1998). Anchizone metamorphism is a transitional zone between diagenesis and true metamorphism where mineral assemblages include illite and chlorite. Epizone metamorphism is characterized by low temperatures and intense deformation.

The quarry is approximately elliptical in plan: 700 m in length (north-south direction), 400 m in width (west-east direction) and 150 m in depth. The overall slope angle varies throughout the pit: 28° at north-east, 40° at east and 50° at north (Shillitto 2013). Coggan and Pine (1996) provided a brief overview of the geology of the quarry and detail of previous discontinuities that have been identified within the quarry slopes. Prominent discontinuities have been given local names by the quarrymen (e.g. Floors, Shortahs and Grain).

Current production at the quarry is limited to the north-east region, where 4-10 m high near-vertical benches are formed by diamond impregnated wire sawing (Figure 2). This excavation technique results in minimal damage to the slate, thereby increasing product recovery. In view of limited rock mass damage the quarry provides an excellent site for investigating rock mass characteristics and potential for discontinuity-controlled instability without having to evaluate the detrimental effects of blast-induced damage to the rock mass. The quarry is currently undertaking a push-back on the upper benches of the north-east region in order to provide access to high quality slate in the central and lower sections of the slope. This is being undertaken using mechanical excavation, with waste material being placed within the west and south regions of the quarry.

Evidence of the potential for discontinuity-controlled instability on the north-east slope can be seen in Figure 3, which shows an image of a recent 50 m wide and 13 m high planar failure on an upper bench. Crack opening was observed by the quarrymen at the crest of the bench during regular inspection and the unstable section safely removed. The basal surface of the failures shown in Figure 3 is provided by Floors with lateral release surfaces provided by Shortahs and Grain. The failures highlight the three-dimensional nature of the potential failure due to blocks formed by the discontinuities and the influence of bench-face orientation on the likelihood for instability.

Previous geological engineering survey have highlighted the controlling influence of discontinuities on both the stability of the quarry and quarrying operations (Clover 1978; Coggan and Pine 1996; Costa et al. 1999). Coggan and Pine (1996) analysed the 1967 failure of the west slope and showed that the failure was controlled by the interaction of several distinct blocks and suggested a progressive multi-

block failure with some degree of block rotation and translation. Costa et al. (1999) carried out a slope stability investigation of the north-east slope to demonstrate the significance of key discontinuities on potential for translational failure. This investigation primarily involved kinematic analysis of specific slope orientations and the use of two-dimensional distinct element modelling with UDEC (Itasca 1997). Previous laboratory direct shear strength tests on several discontinuities from Delabole Slate Quarry, reported in Brown et al. (1977), show that the shear strength of clean surfaces are controlled by water and surface roughness. The average friction angle on smooth wet surfaces is 20.5^o, which is up to 9° less than that of the same surfaces when dry. Surface roughness, however, can add up to 40° to basic friction angles. Brown et al. (1977) also showed that surface roughness features of discontinuities vary markedly with direction and the nature of the discontinuity, giving rise to a wide range of possible shear strengths. Iron staining of discontinuities surfaces causes small increases in friction angles.

We highlight the use and application of several techniques for three-dimensional simulation of the potential for failure of the north/north-east slopes using a combination of:

- Digital data acquisition and subsequent analysis of the point cloud data
- Wedge failure analysis incorporating a basal failure surface
- Application of three-dimensional distinct element modelling to undertake a sensitivity analysis on the key input parameters controlling stability of the modelled slope

Numerical modelling results are presented to show the effects of discontinuity spacing, persistence and shear strength on model behaviour. The procedure for the development, validation and incorporation of a discrete fracture network into a three-dimensional distinct element rock slope model is also outlined.

3. Methodology

Three-dimensional simulation of rock slopes must consider the complexities related to the interaction of 3D slope geometry and true discontinuity set orientations. Slope geometries may often be oversimplified within 3D numerical simulations with little consideration of the potential effects of confinement, slope kinematics, slope curvature and release surfaces. Discontinuities are usually

represented deterministically without accounting for uncertainty and spatial variability which represent inherent characteristics of rock mechanics problems (Einstein and Baecher 1983). Terrestrial remote-sensing techniques (e.g. photogrammetry and laser scanning) now provide a convenient additional tool to help reduce these problems. Photogrammetry and laser scanning provide (x, y, z) point clouds of the slope surface which can be used to build realistic 3D slope geometries. These methods also allow coverage of a wide range of the pit slope surface and the ability to acquire discontinuity databases remotely (Sturzenegger and Stead 2009a). The remote sensing data provides key geotechnical information such as discontinuity orientation and length as well as the location of each joint measurement. The volume of data can be significantly greater both in terms of magnitude and the areal extent mapped compared to traditional geotechnical data mapping (Fekete and Diederichs 2013). The acquired discontinuity data can be used to develop stochastic discrete fracture networks (DFN's) for more realistic representation of discontinuities.

Application of remote sensing methods for discontinuity mapping has increased significantly in the last decade. Coggan et al. (2008), for example, provided a detailed comparison between the results of conventional hand-mapping, terrestrial photogrammetry and laser scanning data (including discontinuity orientation and trace length) for rock mass characterisation. Oppikofer et al. (2009) used terrestrial laser scanning for the structural mapping of the inaccessible main scarp of Åknes rockslide in western Norway. Sturzenegger and Stead (2009b) provided a comprehensive evaluation of terrestrial photogrammetry and laser scanning for discontinuity characterization and presented practical recommendations for optimizing the use of these techniques. Sturzenegger and Stead (2009a) combined terrestrial photogrammetry with laser scanning to generate a 3D model of the South Peak of Turtle Mountain, Alberta, Canada. Firpo et al. (2011) used photogrammetric techniques to obtain geometrical and structural setting of a quarry located in the Carrara Marble District for subsequent distinct element modelling. Tuckey (2012) used photogrammetry and laser scanning to characterize discontinuities in three large open pits (Jwaneng diamond mine, Botswana; Diavik diamond mine, Canada; Highland Valley copper mine, Canada.) and one natural rock slope (Stawamus Chief, Canada). Eyre et al. (2014) showed the application of laser scanning in providing geometrical inputs for subsequent rockfall analysis. These

techniques have also been applied to characterize rock masses underground. Styles et al. (2010) and Preston et al. (2014) used digital photogrammetry to characterize brittle fracture in mine pillars and conducted repeated time-lapse photogrammetry of hard rock pillars in order to characterize changes and damage in rock masses with time.

Discrete fracture network (DFN) generators such as FracMan (Dershowitz et al. 2014) and FracSim3D (Xu and Dowd 2010) can provide a more realistic representation of fractured rock masses. Discrete fracture networks have been used in a wide range of geomechanical problems (e.g. large open pits, tunneling, block caving, reservoir geomechanics, etc.). Elmo and Stead (2010) incorporated a discrete fracture network within the FDEM code, ELFEN (Rockfield 2009), to realistically simulate the behaviour of fractured rock pillars. Vyazmensky et al. (2010) used a combined FDEM/DFN modelling approach to investigate the pit wall instability triggered by caving operations at Palabora mine, South Africa. In order to define a fracture network to represent a natural joint system, at least three sets of parameter are required (Elmo 2006):

- Fracture size distribution

- Fracture orientation distribution

- Fracture density

For flow simulations, fracture transmissivity and aperture should also be defined (Rogers et al. 2006). DFN generator codes such as FracMan consider different parameters (such as areal intensity P_{21} and volumetric intensity P_{32}, Dershowitz et al. 2014) to represent the degree of fracturing in a rock mass. P_{21} and P_{32} are defined as the cumulative length of fractures per unit area and the cumulative area of fractures per unit volume respectively. Rogers et al. (2014) highlighted the importance of the volumetric fracture intensity parameter, P_{32}, in DFN generation as this property represents a non-directional measure of rock mass fracturing, incorporating both fracture frequency and fracture size. They showed that the P_{32} property strongly controls rock mass geomechanical properties such as fragmentation, block size and stiffness.

In this study we use the three-dimensional distinct element code 3DEC V. 5. 0 (Itasca 2014a) to investigate the stability of the north/north-east walls of Delabole Quarry. Figure 4 illustrates the methodology adopted. Terrestrial photogrammetry is performed at the site in order to characterize the rock mass. The point cloud derived from the terrestrial photogrammetry is used to reproduce a realistic 3D slope surface geometry for a section of the north/north-east face which is then incorporated into the numerical simulations using 3DEC. Discontinuity mapping is also performed using the photogrammetry model, allowing development of a realistic discrete fracture network which can be integrated within the 3DEC simulations. The FracMan DFN code is used to determine the statistical parameters that represent the joint sets (i.e. orientations, length and volumetric fracture intensity parameter, P_{32}).

4. Digital data acquisition

In 2012, laser scanning of the quarry was undertaken using a Leica^{TM} ScanStation C10. Strategically placed High Definition Surveying targets and four multi-set-up scan locations were employed to capture the three-dimensional geometry of the north-east face to minimize occlusions (Figure 5). In order to provide later geo-referencing of the scan, differential GPS was also used during the survey with compatible Leica^{TM} SmartScan antennae. Point cloud registration and geo-referencing was performed by Leica^{TM} Geosystems using Leica^{TM} Cyclone software (Leica Geosystems 2010), Figure 6. In 2014, terrestrial photogrammetry was also performed on the north/north-east slopes using a Canon 7D digital camera with a 200 mm focal length lens. The distance between the slope face and camera stations range from 150 to 450 m. The photographs were taken using five camera stations from the bottom of the pit in order to minimize occlusion (Figure 5). The base-distance ratio (the distance between the two camera stations/the average distance to the slope face) was set to 1:5 in order to maximize the calculated distance accuracy. All photographs were processed using the Adam Technology 3DM Analyst software suite (ADAM Technology 2014) including 3DM CalibCam, DTM Generator and 3DM Analyst. In order to georeference the photogrammetry model, control points were selected on the LiDAR model and included within the photogrammetry model. The point cloud obtained from the photogrammetry model served as an input (to generate the slope geometry) for the subsequent slope stability analysis.

The final 3D photogrammetry model and x, y, z, point cloud were then used to map the discontinuities within the pit and to create the 3D slope geometry. Discontinuity surfaces are extracted from the photogrammetry model by fitting a disk to a selected part of the point cloud (Figure 7a). The disk is defined by some key information including a vector normal to the plane, origin (x, y, z) and radius. Structural mapping was conducted on the photogrammetry model and all the mapped discontinuities were imported into Dips V. 6. 0 (Rocscience 2014a) for discontinuity orientation analysis. Figure 7b shows a lower hemisphere equal angle contoured pole plot of the identified discontinuities. Three discontinuity sets (Floors, Grain and Shortahs) were identified within the slope face. Floors dominate the stability of the north-east slope and are associated with numerous low-angle reverse faults which are also responsible for the thickness of the slate in the quarry (Freshney 1972). The remotely captured orientation data compares favorably with previous conventional mapping of discontinuities at the quarry (Table 1).

5. Discrete fracture network development and validation

The discontinuity data from the photogrammetry model (including orientation, location and size) were processed in order to build a representative discrete fracture network. The FracMan code was used to derive the statistical parameters associated with the trace length, orientation as well as the volumetric fracture intensity, P_{32}. The steps undertaken to generate discrete fracture networks for the Delabole Quarry slope are explained below.

5.1. Discontinuity trace length

Discontinuity persistence is typically a key factor in the stability of slopes, yet it is one of the most difficult discontinuity properties to measure. Often long discontinuity traces extend beyond the visible exposure of the rock slope surface, therefore one or both ends of the discontinuity are not visible (Sturzenegger et al. 2007). Therefore, trace length is normally considered as an indication of discontinuity persistence. Values of trace length typically display a Negative Exponential, Power Law or Log Normal distribution, whereby the frequency of very persistent discontinuities is much less than that of less persistent discontinuities (Priest and Hudson 1981; Cai 2011). Elmo (2006) used Log Normal

distributions to describe fracture size distributions from the 2D mapped trace length at the Middleton mine, Derbyshire, UK.

In this study, the Log Normal distribution was found to provide a good fit to the discontinuity trace length data. Figure 8 shows the Log Normal fits assigned to the Cumulative Distribution Function (CDF) plots of trace length for each discontinuity set in order to determine the corresponding trace length distributions. A summary of the statistical parameters that describe the Log Normal distribution of the three discontinuity sets is provided in Table 3.

5.2. Discontinuity orientation

In order to determine the statistical distribution associated with the orientations of the discontinuity sets, the "Interactive Set Identification System" module within the code FracMan is used. This module defines fracture sets from mapping data using an adaptive probabilistic pattern recognition algorithm (Dershowitz et al. 2014). The algorithm defines the orientation distribution for the fractures assigned to each set, and then reassigns fractures to sets according to probabilistic weights proportional to their similarity to other fractures within the set. The orientations of the sets are then recalculated and the process is repeated until the set assignment is optimized (Dershowitz et al. 2014). Using this approach, joint set orientation parameters were fitted to a Fisher distribution and the output parameters used to build a representative DFN. Table 3 shows the statistical parameters that describe the orientations of each discontinuity set.

5.3. Volumetric fracture intensity, P_{32}

P_{32} is the preferred measure for fracture intensity for DFN simulation (Rogers et al. 2014). Unlike P_{10} and P_{21} which can be directly derived from field data (using scanline and window mapping), P_{32} cannot be measured in the field. Dershowitz and Herda (1992) proposed a linear correlation between P_{21} and P_{32} in order to determine P_{32} from P_{21}:

$$P_{32} = C_{21} \times P_{21}$$
Equation 1

Where, C_{21} is a dimensionless constant (constant of proportionality). The value of C_{21} depends on the orientation and size distributions of the joint set as well as the orientations of the outcrop. It is possible

to determine the P_{32} corresponding to the mapped P_{21} in the field by running a series of simulated models and using the fracture size and orientation distributions defined earlier. The basis for this simulated sampling methodology is described in Staub et al. (2002) and Elmo (2006).

Table 2 shows the areal intensity P_{21} values for each discontinuity set as measured from the photogrammetry model, and the corresponding values of C_{21} and P_{32} calculated for the three discontinuity sets using the method described in Staub et al. (2002) . Note that the Floors discontinuity set has the highest P_{21} value (0.14 1/m), while the Shortahs has the lowest value (0.02 1/m). A summary of the statistical parameters that describe the fracture network within the north/north-east slopes is provided in Table 3. These parameters are subsequently used to generate multiple DFN realizations for integration within the 3DEC simulations.

5.4. Discrete fracture network validation

Model validation is an important component of DFN engineering. Since the current DFN model used a simulated sampling methodology to determine fracture intensity P_{32} (i.e. mapped data are already used in the simulated sampling process), validation is consequently limited to the fracture orientation and fracture size. Accordingly, orientations and trace length of the synthetic discontinuities are analysed and compared with the mapped discontinuities (Table 4). Figure 9 shows a lower hemisphere equal angle contoured pole stereoplot of one DFN realization of the three discontinuity sets. The orientations of the stochastically generated discontinuities (Figure 9) compares favorably with the mapped discontinuities (Figure 7b).

In order to validate the Log Normal distributions assigned to the trace length of the three discontinuity sets, a fracture network associated with each discontinuity set is generated in FracMan (using the statistical distributions presented in Table 3). The trace lengths of the synthesized discontinuities on the slope face are then analysed and compared to the trace length analysis for the mapped discontinuities (Figure 8). Figure 10 shows the Cumulative Distribution Function for the trace lengths generated using the DFN representing the three discontinuity sets. By comparing the range of trace lengths and

percentages for the DFN model and the mapped discontinuities, it can be seen that the DFN model favorably reproduces the mapped discontinuities.

6. Block kinematic analysis

Previous studies by Costa et al. (1999) highlight the potential for planar failure to occur on the Floors within the north-east slope depending on bench orientation and shear strength of the discontinuities. Observed instability (shown in Figure 3) suggests that failure may also be influenced by potential lateral release surfaces provided by a number of discontinuities including both the Grain and Shortahs. A preliminary investigation of the kinematics of potential instabilities within the north/north-east slopes was undertaken using Swedge V. 6. 0 (Rocscience 2014b). Within the Swedge model, the Floors discontinuity was considered as a basal failure surface. This analysis examines the possibility of rock slope failure due to the unfavourable orientations of discontinuities. Considering the three discontinuity sets (Floors, Grain and Shortahs) within the model a wedge is formed (Figure 11). The mean values of the discontinuity set orientations (Table 3) are considered in the Swedge model. Shear strength properties within the model are based on the results of laboratory and field tests provided in Costa et al. (1999) for distinct element modelling of the north-east slope (Table 5). Using the shear strength properties shown in Table 5, the wedge is stable with a factor of safety equal to 1.7. Only when the friction angle of the basal surface is decreased to 20° does the model become unstable.

When stability of the rock mass is controlled by displacements along discontinuities, a discontinuum model is the most appropriate tool to investigate the rock mass behaviour. In order to provide a better understanding of slope stability at Delabole Quarry, numerical modelling using the 3D distinct element code, 3DEC (Itasca 2014a), has been performed. 3DEC has been successfully used to investigate the stability of rock structures in both underground and surface applications. For example, Gao (2013) used 3DEC to study the mechanism of roof failures in underground coal mine roadways. Fekete and Diederichs (2013) used combined laser scaning-3DEC modelling for underground rock mass characterization and stability analysis. Salvini et al. (2014) used a DFN-3DEC approach to investigate the stability of a quarry slope located in the Torano basin, Carrara, Italy. They used a combined terrestrial

photogrammetry-laser scanning approach to collect discontinuity data within the quarry. Wolter (2014) used 3DEC to investigate the influence of block geometry and kinematics on failure mechanism of the 1963 Vajont Slide, Italy.

6.1. Distinct element simulation approach

The data gained from the terrestrial photogrammetry of the quarry was used to build the geometry of the slope for 3DEC simulations. The mesh processing code, MeshLab (Cignoni and Ranzuglia 2014) was used to convert the georeferenced photogrammetry point cloud to a 3D surface. This surface was then converted into a closed volume using the Rhinoceros code (McNeel 2014). Finally the closed volume was prepared for input into 3DEC using KUBRIX® Geo (Itasca 2014b) for the subsequent distinct element simulations. The model vertical lateral boundaries were fixed in the horizontal direction and the base of the model fixed in both the horizontal and vertical directions. A network of history points comprising five columns and six rows (30 points in total) was located within the model to monitor displacements and velocities throughout the slope simulations. Such an extensive slope monitoring method is designed to better understand the behaviour and stability of different parts of the modelled slope with increasing calculation time steps. In 3DEC, blocks can behave as either rigid or deformable with an assumed stress–strain constitutive criteria (Cundall 1988). Due to the relatively shallow depth of the quarry (150 m) and the discontinuity controlled nature of the observed instabilities, rigid blocks (with 2600 kg/m^3 density) were assumed in order to focus the investigation on the influence of block kinematics and the strength properties of discontinuities on potential failure mechanisms. Two different discontinuum approaches were used in this study:

1. The discontinuity sets from the stereonet analysis (Figure 7b) were used to develop the geomechanical model and the effect of change in friction angle, spacing and persistence of the joint sets investigated through a series of parametric analyses.

2. Multiple realizations of discrete fracture networks were built based on the results presented in section 5 and integrated within the 3DEC model.

6.2. Deterministic approach

6.2.1. Influence of the friction angle of the modelled basal surface (Floors)

Kinematic analysis using Swedge suggested that the potential for sliding on Floors is controlled by the discontinuity shear strength. Therefore, using a parametric analysis approach, the influence of the friction angle on the stability of the slope was investigated in 3DEC. Three discontinuity sets were assumed within the model, however, only friction angle of the basal surface (Floors) was varied in the simulations. Shear strength and spacing of the joint sets are presented in Table 5. Figure 12 shows 3DEC results for specific model runs with different friction angle values assumed for the Floors. It should be noted that all models were run for 200000 calculation time steps. Based on the assumed slope geometry and discontinuity sets, model instability is considered in terms of localized and inter-ramp failure. With reduction in the friction angle of the Floors set from 31° to 26°, a minor failure simulated which is limited to the bench scale, involving block translational and block rotational modes of failure (as shown in Figure 12a). Further reduction in the friction angle, increases the extent of the simulated slope failure to the inter-ramp scale (Figure 12b, c and d). Block failures within the models occur through opening along Shortahs, lateral shear along Grain and sliding on the Floors discontinuity sets (Figure 12d). It is also evident that the north-east part of the simulated slope is more unstable than the north section. This is in good agreement with field observations, and emphasizes the controlling influence of discontinuity orientation relative to slope face orientation on potential instability. Since the dip direction of the Floors is within ±20° of the dip direction of the north-east slope, this part of the model is more susceptible to discontinuity-controlled instability. The dip direction of the north part of the model, however, is significantly different from the Floors, resulting in increased stability within the model.

Figure 13 shows the increase in displacements throughout the model at different calculation time steps. Each cell represents a history point located within the model as defined in Figure 12a. The value within the cell represents the maximum horizontal displacement of the history point at the specified time step. The displacement values are colour-coded (with green representing low displacement values and red representing higher displacement values). This methodology provides improved visualization of both the

extent and magnitude of displacements throughout the slope simulation process in different parts of the slope. This "spatio-temporal" displacement plot clearly shows the development of instability zones within the north-east slope. Horizontal displacements in the models are compared and illustrated in Figure 14. From this it is evident that the instability within the models decreases with a reduction in the friction angle of the Floors joint set.

6.2.2.   Influence of discontinuity set spacing

A second series of 3DEC simulations was undertaken to investigate the effect of discontinuity set spacing on the potential slope failure mechanism. For these models, the friction angle of the basal surface was maintained at 22°. Four 3DEC models with increased spacing values were investigated. In these models, the original spacing values provided in Table 5 were multiplied by 2, 3 and 4 (Table 6). This was undertaken to maintain the observed in-situ relative block size aspect/dimensions. With an increase in spacing value by a factor of two, failure occurs at the inter-ramp scale (Figure 15b). When the spacing value is multiplied by a factor of three, failure occurs at the bench scale only with a significant decrease in the number of blocks involved (Figure 15c). Individual block failures only occur in the north-east part of the slope. A further increase in spacing (when multiplied by four) results in no significant displacements within the model, and the model appears fully stable (Figure 15d). Plots of horizontal displacements versus calculation time steps also show an increase in the model stability with increase in assumed joint spacing, highlighting the influence of modelled block size on model behaviour (Figure 16).

6.2.3.   Influence of discontinuity persistence on modelled slope behaviour

The effect of non-persistent discontinuities and intact rock bridges on the stability of rock slopes has been emphasized within the literature (e.g. Tuckey et al. 2012; Havaej et al. 2012). Due to the inherent difficulties in the measurement of persistence, a parametric analysis assuming a range of persistence values may provide an improved understanding of the slope behaviour when discontinuities are not fully persistent (as often the case in rock engineering problems).

In 3DEC persistence can be assigned to discontinuities as a probability that any given block lying in the path of a joint will be split (Itasca 2014a). For example, if a persistence value equal to 0.9 (p = 0.9) is

assigned to a discontinuity, then on average 90% of the blocks will be split. (Brideau et al. 2012) used this method to investigate the effect of persistence on the stability of a concave rock slope. In this section we investigate the influence of persistence of the three discontinuity sets on the slope failure mechanism in the north-north east face of Delabole Quarry. The persistence value assigned to the basal surface is shown in Table 7. Block movements for the model assuming a fully persistent basal surface (p=1) were previously illustrated in Figure 12c. Decreasing the p-value to 0.8 significantly decreases the extent of failure particularly at the top of model (Figure 17a). The 3DEC slope model remains unstable at most of the benches (especially within the north-east section of the modelled slope). A further reduction in the scale of the failure is observed when the persistence value is further reduced to 0.6 (Figure 17b). Limited bench scale failure is observed when the p-value is decreased to 0.4 (Figure 17c), and no unstable blocks are formed when the p-value is decreased to 0.2 (Figure 17d). The recorded horizontal displacements for all the persistence models are presented in Figure 18. Models 2-4 show a continuous increase in the recorded displacements while model 5 is stable with insignificant horizontal displacements, highlighting the controlling influence of modelled persistence on slope behaviour.

6.3. Stochastic simulations using discrete fracture networks in 3DEC

Using the statistical parameters associated with the three discontinuity sets (Table 3), we developed discrete fracture networks which were then incorporated within the 3DEC models. Due to the stochastic description of the joint system, each 3DEC model has a unique realization of discontinuities therefore each generated DFN is slightly different. In this study four DFN realizations are generated and simulated in 3DEC (Figure 19). A visual comparison between the results of the DFN models and the previous deterministic models shows a similar type of failure mechanism with planar failure on the Floors and lateral release provided by the Grain and Shortahs. This highlights the detrimental effect of Floors on the stability of the model, particularly within the north-east part of the quarry. Figure 20 compares the block shapes and sizes in the stochastic models (Figure 19) and the initial deterministic model (Figure 12c). While the failed blocks within the deterministic model are formed by tetrahedral and pentahedral wedges (ranging in size from 4 to 8 meters), shapes of the failed blocks within the stochastic models vary from tetrahedral and pentahedral wedges to polyhedral and columnar blocks (ranging in size from

1 to 10 meters). This provides an improved indication of the in-situ variability of block shapes and sizes observed in the north-east slope of the quarry. Similar to the deterministic models, the majority of the failed blocks are located within the northern and north-eastern parts of the quarry slope. In order to better understand the stability of each DFN realization, using the same methodology as in section 6.2.1 (Figure 13e), displacements throughout the models are recorded and presented using a colour coding approach (Figure 21). The displacement plot of realization 3 shows failure of only one history point while realizations 1, 2 and 4 show failure of several history points. It should be noted that due to the relatively large distances between the history points, some of the block failures (in between history points) may not by recorded by the history points. Realization 4 shows the highest displacement value (5.2 meters) within the four realizations.

Depending on the kinematics and relative orientation of discontinuities that surround a failing block, different failure behaviour may occur. In order to further our understanding on the failure mechanism of the failed blocks, inverse numerical velocity and horizontal displacement plotted against time steps can be used. This "inverse velocity" method is often used in displacement monitoring practices to predict the time of failure. Using this method the stability of a moving slope is assessed by defining if monitored velocity data indicates that the slope movement is regressive or progressive (Zavodni and Broadbent 1980; Mercer 2006; Dick et al. 2013). A regressive movement is periodic deceleration of the slope leading to a stable slope while a progressive movement displays accelerating displacements leading to slope collapse. In this method, the point at which the behaviour of the slope changes from regressive to progressive is called "onset-of-failure". Figure 22 compares inverse numerical velocity plots for realization 1 (history point 23) and realization 2 (history point 17). The onset-of-failure in the 3DEC model coincides with the point at which the inverse velocity plot starts approaching zero and subsequent displacements continuously increase. Although the onset-of-failure for both models occurs at 10000 calculation time steps, the progressive part of the two plots exhibit two distinct behaviours. The horizontal displacement plot of realization 1 exhibits a relatively smooth increase and the inverse velocity plot shows a relatively smooth decrease towards zero indicating the complete kinematic freedom of the failing block. In realization 2 however, the downward trend of inverse velocity and

upward trend of horizontal displacement are interrupted in two instances (time steps 32800 and 53800). This indicates a relative degree of block confinement and interlocking in the vicinity of the failing block prohibiting continuous displacement of the block. Figure 23 explains the clear differences in the failure mechanism and inverse velocity plots of the failing blocks in realizations 1 and 2. Due to their kinematic freedom, the failing blocks in realization 1 are continuously moving out of the slope while the movements of the failing blocks in realization 2 are slowed and constrained by confinement and interlocking caused by displacements of the neighbouring blocks. This inter-relation between slope failure, kinematics and inverse velocity plots has been previously observed in numerical simulation of natural and engineered slopes using Slope Model (Itasca 2010), a 3D brittle fracture code (Havaej et al. 2014 and Havaej et al. Submitted).

7. Conclusions

Digital data acquisition has been successfully used to collect discontinuity characteristics for the north-east slope of Delabole Slate Quarry. Using this technique we were able to produce an accurate data set which includes key discontinuity properties such as orientation, trace length and the location of each discontinuity measurement. This extensive data set was then used to statistically describe the variability of discontinuity orientation, length and intensity through development of discrete fracture networks. Incorporation of these DFNs into a realistic 3D slope geometry of the Delabole Quarry developed from the photogrammetry point cloud, helped to better understand the influence of discontinuity variability, kinematics and slope curvature on the potential failure mechanism of the rock slope.

Stereonet analysis of the remotely captured orientation data set resulted in identification of three discontinuity sets (Floors, Shortahs and Grains). Mean dip and dip direction of the three discontinuity sets agrees favourably with previous hand mapping undertaken at the quarry. Swedge analysis, using the newly-released basal wedge emphasized the potential for sliding on Floors with lateral release surfaces provided by both Shortahs and Grain, agreeing with field observations.

Deterministic 3DEC simulations were initially used to investigate the influence of the three discontinuity sets on the stability of the slope face. A series of parametric analyses considering the influence of

41

friction angle, spacing and persistence of the discontinuities on model behaviour was conducted. The results highlighted the critical role these parameters have on potential for instability, and the probable extent of modelled failure in the north-east slope at Delabole.

Stochastic simulations, using a combined 3DEC-DFN approach, showed a broader range of failed block shapes and sizes within the modelled rock slope (Figure 20). This better captures the observed variability of block failures within the north-east slope of the Delabole Quarry. Both the deterministic and stochastic models showed instabilities in the north/north-east part of the slope while the north-west part was more stable.

Application of a spatio-temporal displacement analysis provides considerable potential for improved understanding of the behaviour of rock slope deformation. Application of the inverse velocity approach (commonly used in displacement monitoring practices) provided a better understanding on the modelled failure mechanisms of the failed blocks. It also helped to determine the numerical onset-of-failure. This is particularly important since failure in a numerical model is often associated with selected but somewhat arbitrary displacement values. The onset-of-failure method provides a more rigorous methodology to define the numerical time of failure within the simulations.

8. Acknowledgments

9. References

ADAM Technology. (2014). *3DM Analyst Mine Mapping Suite*. ADAM Technology, Belmont, Australia.

Brideau, M. A., Chauvin, S., Andrieux, P., and Stead, D. (2012). Influence of 3D statistical discontinuity variability on slope stability conditions. *Landslides and Engineered Slopes: Protecting Society through Improved Understanding*, Banff, Canada, 587–593.

Brown, E.T, Richards, L.R. and Barr, M.V. (1977). Shear strength characteristics of the Delabole Slates. Conference on Rock Engineering, Newcastle-upon-Tyne, UK, April 4-7, 33-51.

Cai, M. (2011). Rock mass characterization and rock property variability considerations for tunnel and cavern design. *Rock Mechanics and Rock Engineering*, 44(4), 379–399.

Cignoni, P., and Ranzuglia, G. (2014). MeshLab, a mesh processing system, for user assisted editing. *Visual computing lab - ISTI -CNR*.

Clover, A. W. (1978). Some aspects of the rock excavations on the western face at Delabole Slate Quarry, Cornwall. MSc Thesis, Imperial College, University of London, London, UK.

Coggan, J., Gwynn, X. P., Pine, R. J., and Wetherelt, A. (2008). Rock mass characterisation: is there a role for remote mapping techniques ? *Remote Sensing and Photogrammetry Society Conference*, Exeter, UK, 4 Pages.

Coggan, J. S., and Pine, R. J. (1996). Application of distinct-element modelling to assess slope stability at Delabole slate quarry, Cornwall, England. Transactions of the Institution of Mining and Metallurgy. Section A. Mining Industry 105, A22–A30.

Costa, M., Coggan, J. S., and Eyre, J. M. (1999). Numerical modelling of slope behaviour of Delabole slate quarry (Cornwall, UK). *International Journal of Surface Mining, Reclamation and Environment*, 13(1), 11–18.

Cundall, P. A. (1988). Formulation of a three-dimensional distinct element model—Part I. A scheme to detect and represent contacts in a system composed of many polyhedral blocks. *International Journal of Rock Mechanics and Mining Sciences & Geomechanics Abstracts*, 25(3), 107–116.

Dershowitz, W. S., and Herda, H. (1992). Interpretation of fracture spacing and intensity. *42nd U.S. Rock Mechanics/Geomechanics Symposium*, American Rock Mechanics Association, Santa Fe, New Mexico., 8 pages.

Dershowitz, W. S., Lee, G., Geier, J., and LaPointe, P. (2014). FracMan: interactive discrete feature data analysis, geometric modeling and exploration simulation. Golder Associates Inc.

Dick, G. J., Eberhardt, E., Stead, D., and Rose, N. D. (2013). Early detection of impending slope failure in open pit mines using spatial and temporal analysis of real aperture radar measurements. *Slope Stability 2013*, Australian Centre for Geomechanics, 949–962.

Einstein, H. H., and Baecher, G. B. (1983). Probabilistic and statistical methods in engineering geology. *Rock Mechanics and Rock Engineering*, 16(1), 39–72.

Elmo, D. (2006). Evaluation of a hybrid FEM/DEM approach for determination of rock mass strength using a combination of discontinuity mapping and fracture mechanics modelling, with particular emphasis on modelling of jointed pillars. Ph.D., University of Exeter, Exeter, UK.

Elmo, D., and Stead, D. (2010). An integrated numerical modelling–discrete fracture network approach applied to the characterisation of rock mass strength of naturally fractured pillars. *Rock Mechanics and Rock Engineering*, 43(1), 3–19.

Eyre, M. L., Pascoe, D., Patrick, F., and Coggan, J. (2014). Digital data acquisition for effective slope management. *22nd UK Conference of the Association for Computational Mechanics in Engineering*, Exeter, UK, 4 pages.

Fekete, S., and Diederichs, M. (2013). Integration of three-dimensional laser scanning with discontinuum modelling for stability analysis of tunnels in blocky rockmasses. *International Journal of Rock Mechanics and Mining Sciences*, 57, 11–23.

Firpo, G., Salvini, R., Francioni, M., and Ranjith, P. G. (2011). Use of Digital Terrestrial Photogrammetry in rocky slope stability analysis by Distinct Elements Numerical Methods. *International Journal of Rock Mechanics and Mining Sciences*, 48(7), 1045–1054.

Freshney, E. C. (1972). *Geology of the coast between Tintagel and Bude: (Explanation of part of one-inch geological sheet 322, new series)*. Her Majesty's Stationery Office, London.

Gao, F. (2013). Simulation of failure mechanisms around underground coal mine openings using discrete element modelling. PhD Thesis, Simon Fraser University, Burnaby, Canada.

Havaej, M., Stead, D., Lorig, L., and Vivas, J. (2012). Modelling rock bridge failure and brittle fracturing in large open pit rock slopes. *46th U.S. Rock Mechanics/Geomechanics Symposium*, American Rock Mechanics Association, Chicago, Illinois, 9 pages.

Havaej, M., Stead, D., Mayer, J., and Wolter, A. (2014). Modelling the relation between failure kinematics and slope damage in high rock slopes using a lattice scheme approach. *48th U.S. Rock Mechanics/Geomechanics Symposium*, American Rock Mechanics Association, Minneapolis, Minnesota, 8 pages.

Havaej, M., Wolter, A., and Stead, D. (Submitted). Exploring the potential role of brittle rock fracture in the 1963 Vajont Slide, Italy. *International Journal of Rock Mechanics and Mining Sciences*.

Itasca. (1997). *UDEC 3.0. manual*. Itasca Consulting Group Inc., Minneapolis, United States.

Itasca. (2010). *Slope Model, description of formulation with verification and example problems. Revision 2.* Itasca Consulting Group Inc., Minneapolis, United States.

Itasca. (2014a). *3DEC-3 dimensional distinct element code user's guide*. Itasca Consulting Group Inc., Minneapolis, United States.

Itasca. (2014b). *KUBRIX Geo, advanced automatic and interactive grid generation for engineering software*. Itasca Consulting Group Inc., Minneapolis, United States.

Leese, C. E., and Setchell, J. (1937). *Notes on Delabole slate quarry.* Trans. Roy. Geol. Soc., Cornwall, UK, 17, 41–7.

Leica Geosystems. (2010). *Leica Cyclone; 3D point cloud processing software*. Leica Geosystems HDS, Heerbrugg, Switzerland.

McNeel. (2014). *Rhinoceros, modelling tool for designers*. McNeel North America.

Mercer, K. G. (2006). Investigation into the time dependent deformation behaviour and failure mechanisms of unsupported rock slopes based on the interpretation of observed deformation behaviour. PhD Thesis, University of the Witwatersrand.

Oppikofer, T., Jaboyedoff, M., Blikra, L., Derron, M.-H., and Metzger, R. (2009). Characterization and monitoring of the Åknes rockslide using terrestrial laser scanning. *Nat. Hazards Earth Syst. Sci.*, 9(3), 1003–1019.

Preston, R., Roberts, D., McIntire, H., and Stead, D. (2014). Use of photogrammetry and discrete fracture networks to characterize pillar damage and rock mass characteristics. *International discrete fracture network engineering conference*, Vancouver, Canada, 11 pages.

Priest, S. D., and Hudson, J. A. (1981). Estimation of discontinuity spacing and trace length using scanline surveys. *International Journal of Rock Mechanics and Mining Sciences & Geomechanics Abstracts*, 18(3), 183–197.

Riggs, W. H. H. (2014). Applications of thermal imaging in mining and coastal slope stability analysis. MSc Thesis, The University of Exeter, Penryn, UK.

Rockfield. (2009). *ELFEN manual version 4.4.* Rockfield Software Limited, Swansea, UK.

Rocscience. (2014). *Dips 6.0, graphical and statistical analysis of orientation data*. Rocscince Inc., Toronto, Canada.

Rogers, S., Elmo, D., Webb, G., and Catalan, A. (2014). Volumetric fracture intensity measurement for improved rock mass characterisation and fragmentation assessment in block caving operations. *Rock Mechanics and Rock Engineering*, 1–17.

Rogers, S., Moffitt, K., and Kennard, D. T. (2006). Probabilistic slope and tunnel block stability analysis using realistic fracture network models. *Golden Rocks 2006 The 41st U.S. Symposium on Rock Mechanics (USRMS)*, 8 pages.

Salvini, R., Giovannini, R., Vanneschi, C., Riccucci, S., Francioni, M., and Stead, D. (2014). The use of remote sensing for discontinuity mapping and analysis in a large marble quarry, Carrara, Italy. *International discrete fracture network engineering conference*, Vancouver, Canada, 11 pages.

Selwood, E.B., Thomas, J.M., Williams, B.J., Clayton, R.E., Durning, B., Smith, O. and Warr, L.N. (1998). Geology of the country around Trevose Head and Camelford. British Geological Society, 101 pages.

Shillitto, D. A. (2013). Delabole quarry - geotechnical assessment and pit design of the north east sector. MSc Thesis, The University of Exeter, Penryn, UK.

Staub, I., Fredriksson, A., and Outters, O. (2002). *Strategy for a rock mechanics site descriptive model development and testing of the theoretical approach*. Swedish Nuclear Fuel and Waste Management Co, Stockholm Sweden, 219 pages.

Sturzenegger, M., and Stead, D. (2009a). Quantifying discontinuity orientation and persistence on high mountain rock slopes and large landslides using terrestrial remote sensing techniques. *Nat. Hazards Earth Syst. Sci.*, 9(2), 267–287.

Sturzenegger, M., and Stead, D. (2009b). Close-range terrestrial digital photogrammetry and terrestrial laser scanning for discontinuity characterization on rock cuts. *Engineering Geology*, 106(3–4), 163–182.

Sturzenegger, M., Yan, M., Stead, D., and Elmo, D. (2007). Application and limitations of ground-based laser scanning in rock slope characterization. American Rock Mechanics Association, Vancouver, Canada, 29–36.

Styles, T. D., Zhang, Y., and Stead, D. (2010). A photogrammetric approach to brittle fracture characterization in mine pillars. *44th U.S. Rock Mechanics/Geomechanics Symposium*, American Rock Mechanics Association, Salt Lake City, Utah, United States, 8 pages.

Tuckey, Z. (2012). An integrated field mapping-numerical modelling approach to characterising discontinuity persistence and intact rock bridges in large open pit slopes. MSc Thesis, Simon Fraser University, Burnaby, Canada.

Tuckey, Z., Stead, D., Havaej, M., Gao, F., and Sturzenegger, M. (2012). Towards an integrated field mapping-numerical modelling approach for characterising discontinuity persistence and intact rock bridges in large open pits. *The Canadian Geotechnical Society (Geo Manitoba)*, Winnipeg Manitoba, 15 pages.

Vyazmensky, A., Stead, D., Elmo, D., and Moss, A. (2010). Numerical analysis of block caving-Iinduced instability in large open pit slopes: A finite element/discrete element approach. *Rock Mechanics and Rock Engineering*, 43(1), 21–39.

Wolter, A. (2014). Characterisation of large catastrophic landslides using an integrated field, remote sensing and numerical modelling approach. PhD Thesis, Simon Fraser University, Burnaby, Canada.

Xu, C., and Dowd, P. (2010). A new computer code for discrete fracture network modelling. *Computers & Geosciences*, 36(3), 292–301.

Zavodni, Z. M., and Broadbent, C. D. (1980). Slope failure kinematics. *Bulletin Canadian Institute of Mining, Canadian Institute of Mining and Metallurgy*, 73, 69–74.

Table 1. Orientation of discontinuity sets within the north-east slope of the Delabole Quarry compared to the previous measurements

Discontinuities	Clover (1978)		Rosthorn (1991)		Costa et al. (1999)		Current data	
	Dip (°)	Dip direction (°)	Dip (°)	Dip direction (°)	Dip (°)	Dip direction (°)	Dip (°)	Dip direction (°)
Floors	20-30	225	35	247	52	253	16	264
Grain	75	055	84	296	72	031	74	022
Shortahs	75	100	73	106	73	94	73	105

Table 2. Measured fracture intensity values (P_{21}) for the three joint sets and determined C_{21} and P_{32} values

Discontinuity set	P_{21} (1/m)	C_{21}	P_{32} (1/m)
Floors	0.14	1/0.3 = 3.3	0.46
Grain	0.03	1/0.81 = 1.23	0.037
Shortahs	0.02	1/0.9 = 1.1	0.022

Table 3. Summary of the statistical parameters that describe the fracture system within the north, north-east slopes of Delabole Quarry

Discontinuity set	Properties	Distribution	Parameters
Floors	Length(m)	Log Normal	Mean: 0.8 deviation: 0.6
	Orientation (°)	Fisher	Dip 16, Dip direction 270, κ 18
	P_{32} (1/m)		0.46
Grain	Length(m)	Log Normal	Mean: 0.4 deviation: 0.4
	Orientation (°)	Fisher	Dip 64, Dip direction 16, κ 8

	P$_{32}$ (1/m)		0.037
Shortahs	Length(m)	Log Normal	Mean: 0.1 deviation: 0.6
	Orientation (^{o})	Fisher	Dip 70, Dip direction 110, к 10
	P$_{32}$ (1/m)		0.022

Table 4. Mean dip and dip directions of the three discontinuity sets obtained from the photogrammetry and DFN models

Discontinuity set	Photogrammetry		DFN	
	Dip (°)	Dip direction (°)	Dip (°)	Dip direction (°)
Floors	16	264	16	267
Grain	74	22	69	19
Shortahs	73	105	74	109

Table 5. Geomechanical properties and spacing of discontinuity sets within the north/north-east slopes of Delabole Quarry (Costa et al. 1999)

Parameter	Floors	Grain	Shortahs
Cohesion (MPa)	0	0	0
Friction angle (°)	31	41	41
Dilation angle (°)	10	5	5
Normal stiffness (GPa/m)	7	12	12
Shear stiffness (GPa/m)	0.7	1.2	1.2
Spacing (m)	3	15	5

Table 6. Spacing of discontinuities used in each numerical model

Spacing multiplier	Floors (m)	Grain (m)	Shortahs (m)
1-initial spacing	3	15	5
2	6	30	10
3	9	45	15
4	12	60	20

Table 7. Varied persistence of the three discontinuity sets

Model No.	Persistence (%)
1-Initial persistence	100
2	80
3	60
4	40
5	20
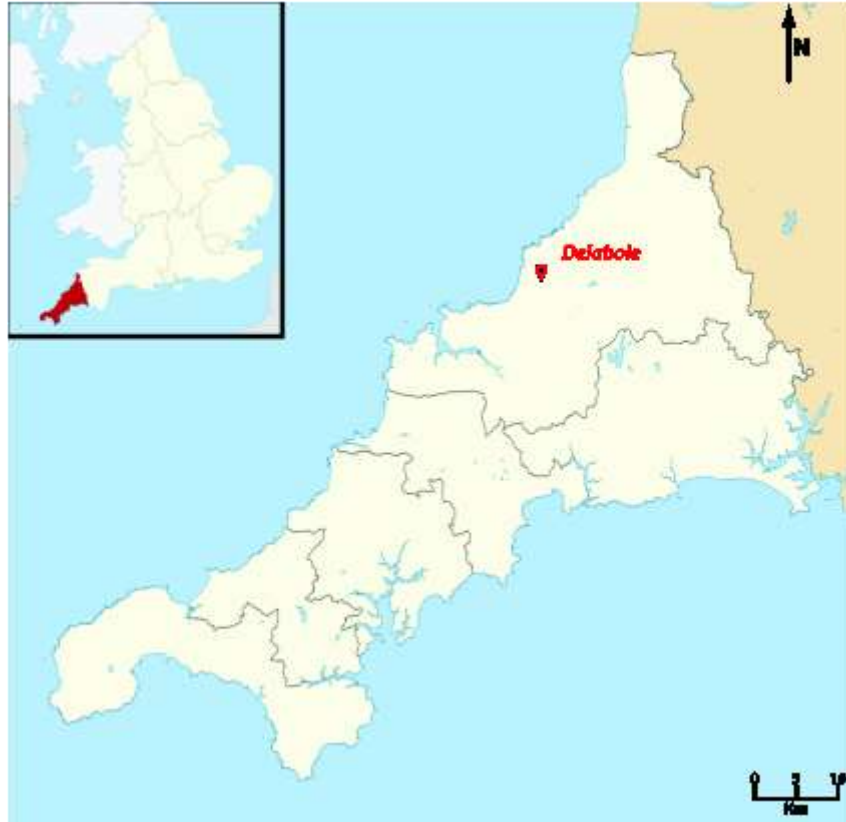
Figure 1. Delabole Slate Quarry located in Cornwall, United Kingdom (source: Ordnance Survey; http://www.ordnancesurvey.co.uk/)

Figure 2. Photograph of the north/north-east slope taken from the south of Delabole Quarry looking north; overall slope height is approximately 150 meters, bench heights are between 4 to 10 meters

Figure 3. The 2012 planar failure on the upper bench of north-east Delabole Quarry slope and showing the discontinuity sets that caused the failure; the strike length of upper section of the failure is 50 m
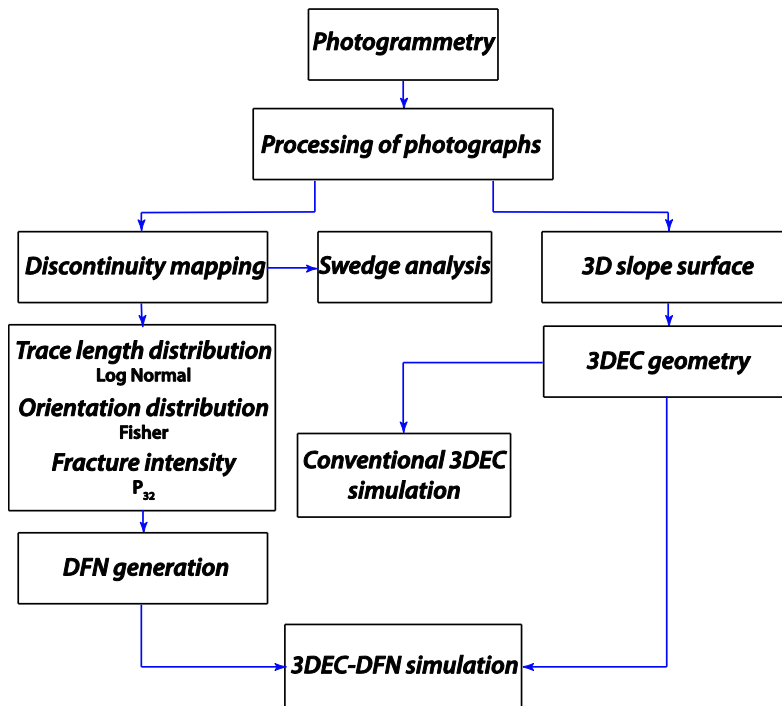
Figure 4. Methodology adopted for rock mass characterization and subsequent numerical simulations
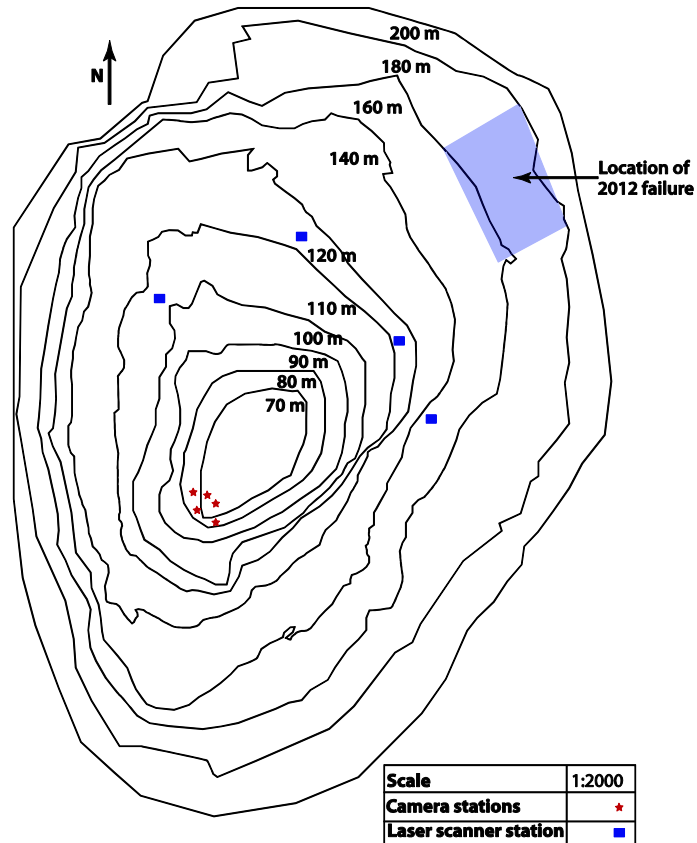
Figure 5. Plan view of Delabole Slate Quarry illustrating the locations of camera and laser scanner stations (after Shillitto 2013)

Figure 6. Example screen-shot image of a section of the geo-referenced x, y, z point cloud based on 2012 laser scanning (the scale bar is indicative only)

a

Floors

Grain

Shortahs

C

Shortahs
73⁰/105⁰

Floors
16⁰/264⁰

Grain
74⁰/022⁰
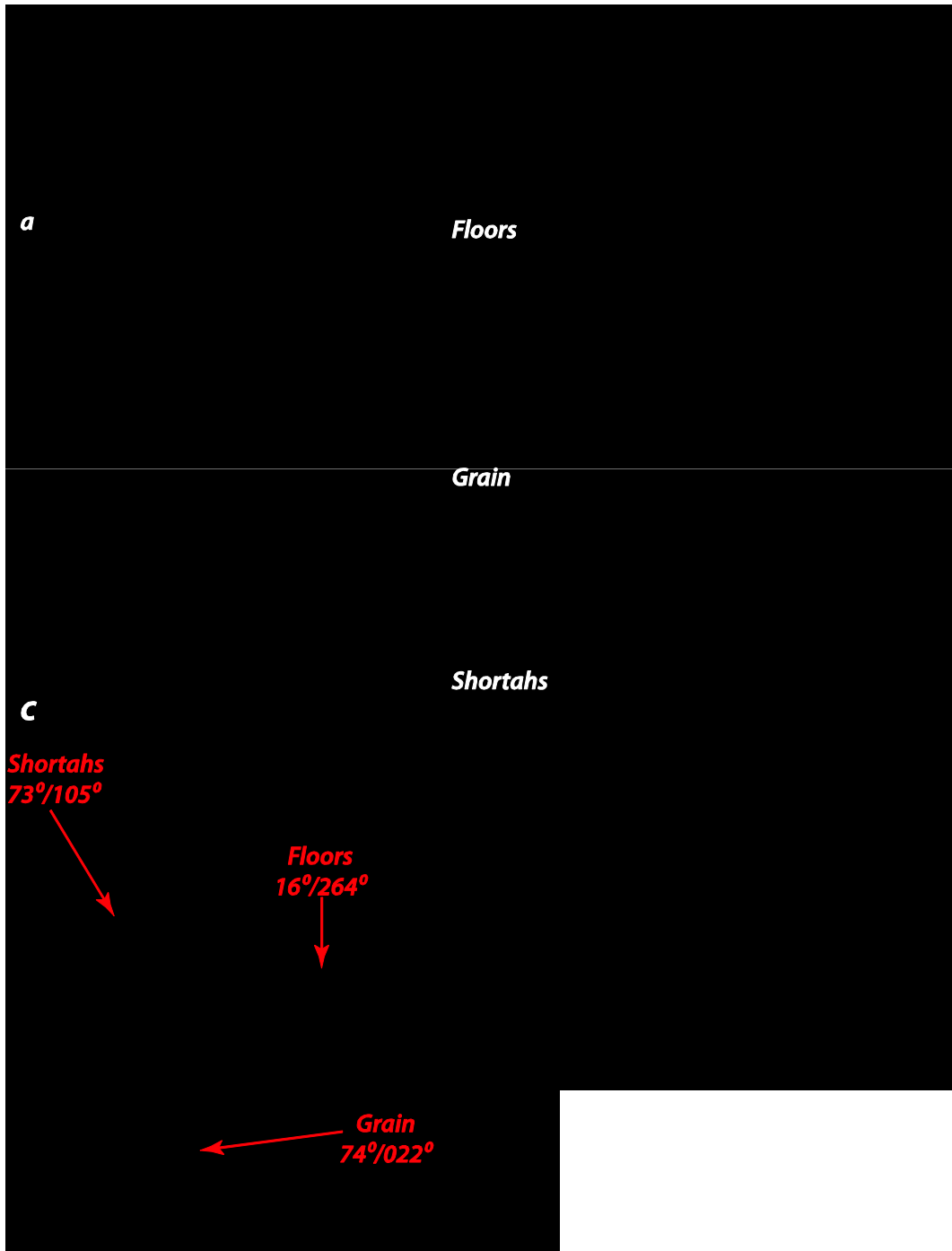
Figure 7. a. Discontinuity mapping of the North-North East face of Delabole quarry using the photogrammetry model; each disc represents a discontinuity measurement, b. Lower hemisphere equal angle contoured pole plot showing the three discontinuity sets within the Delabole Quarry North-North East slope face.
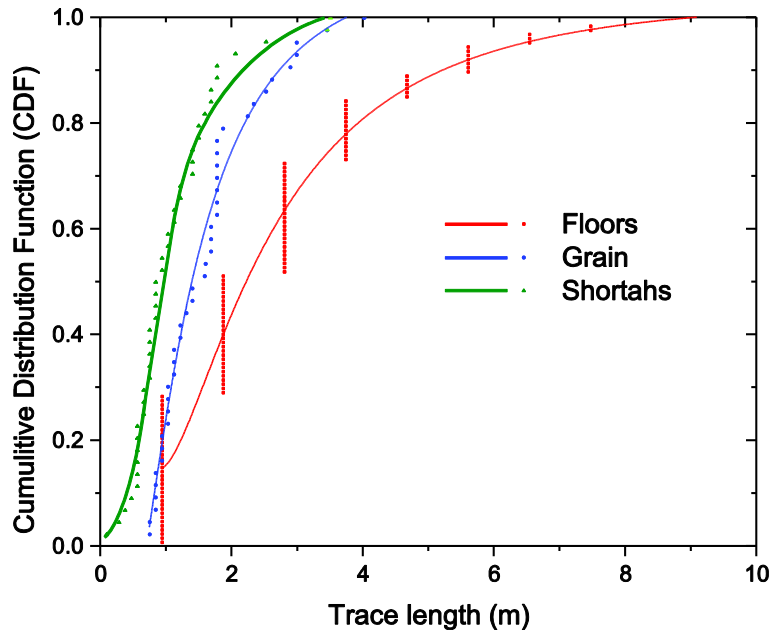
Figure 8. Cumulative Distribution Function of trace lengths for the three discontinuity sets (Floors, Grain and Shortahs) and Log Normal fit assigned to the data (each dot represents a discontinuity measurement and the lines show the Log Normal fit assigned to the data)
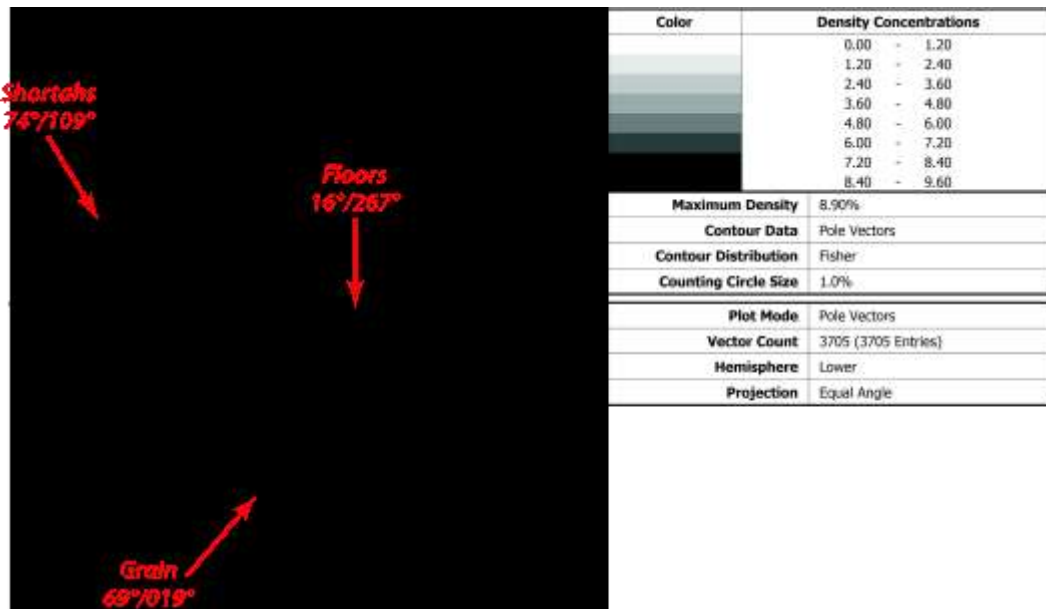
Figure 9. Synthetic joint orientation data using the statistical parameters that describe the fracture system (Table 3)

56
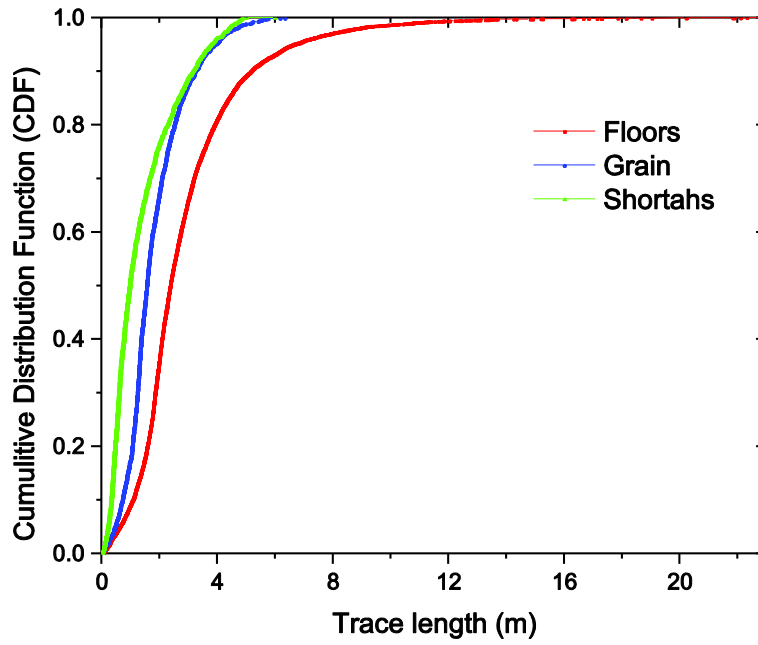
Figure 10. Cumulative Distribution Function of trace length of the three discontinuity sets (Floors, Grain and Shortahs) generated using the using the statistical parameters described in Table 3.Table 3
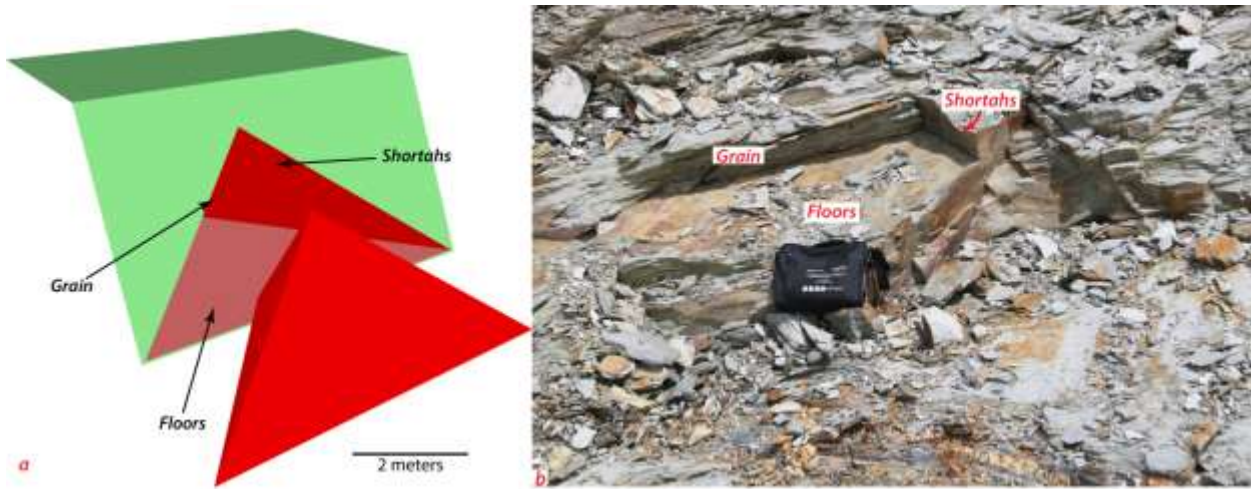
Figure 11. a. Swedge model illustrating a socket wedge formed by the three discontinuity sets (Floors, Grain and Shortahs); b. a small scale discontinuity controlled failure within the quarry slope
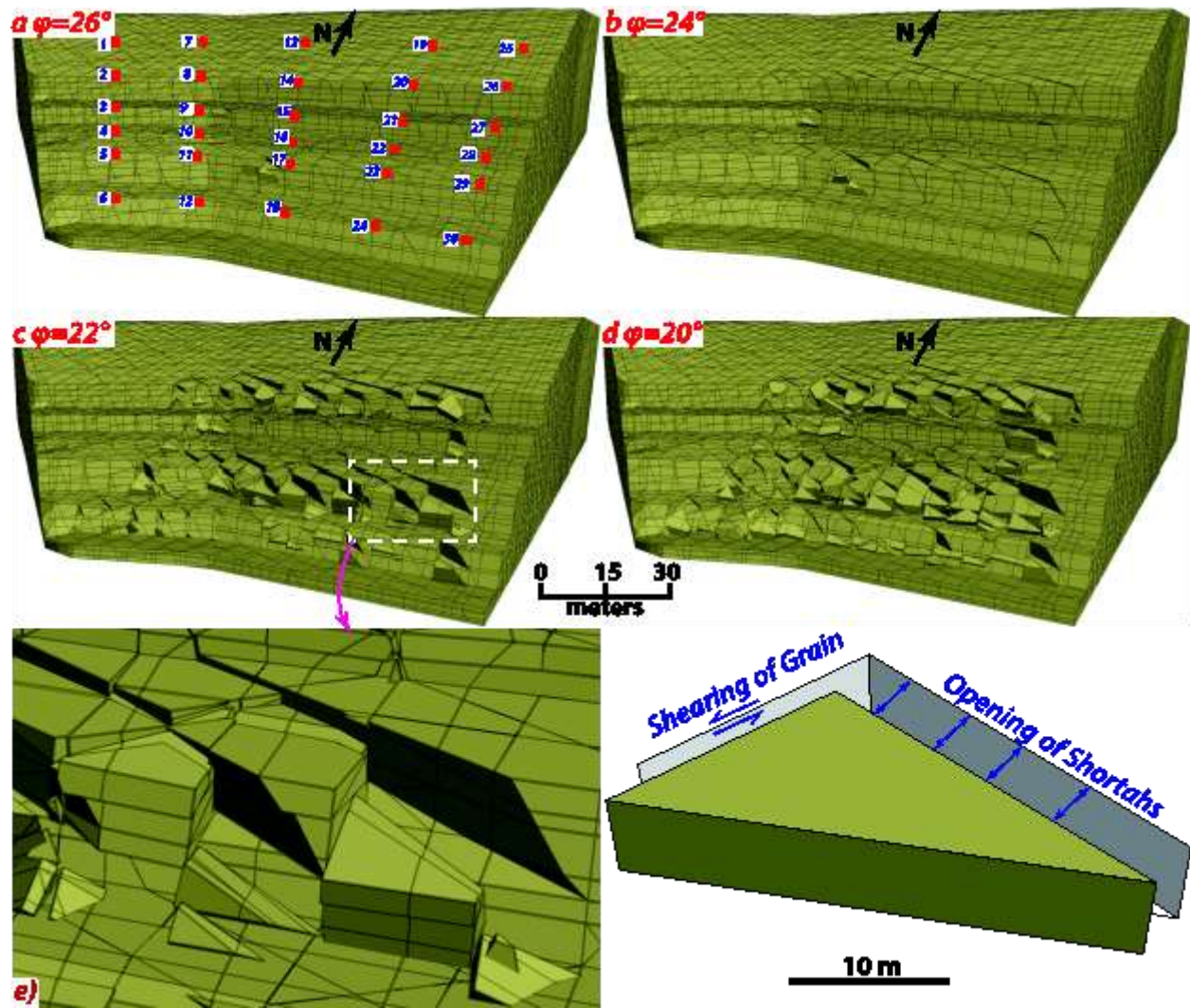
Figure 12. a. location of the network history monitoring points; failure of 3DEC models with varied friction angle of the basal surface (Floors); a. 26°, b. 24°, c. 22° and d. 20°; e. Inset illustrating the failure mechanism, opening of Shortahs and shearing along Grain and Floors discontinuities

20000 steps					40000 steps				
0	0	0	0	0	0	0	0	0	0
0	0	0	0.1	0.1	0	0	0	0.5	0.4
0	0	0	0.1	0	0	0	0	0.2	0.1
0	0	0	0.1	0	0	0	0	0.2	0
0	0.1	0.1	0.1	0.1	0	0.4	0.4	0.4	0.3
0.1	0.1	0	0	0	0.3	0.2	0	0	0.1
60000 steps					80000 steps				
0	0	0	0	0	0	0	0	0	0
0	0	0	1.1	1.1	0	0	0	2	1.7
0	0	0	0.4	0.3	0	0	0	0.7	0.5
0	0	0	0.3	0	0	0	0	0.5	0
0	0.9	1	0.1	0.7	0	1.6	1.8	1.8	1.3
0.6	0.5	0	0	0.3	1.1	0.9	0	0	0.6
100000 steps					120000 steps				
0	0	0	0	0	0	0	0	0	0
0	0	0	2.8	2.1	0	0	0	3	2.1
0	0	0	1	0.7	0	0	0	1	0.7
0	0	0	0.6	0	0	0	0	0.7	0
0	2.3	2.6	2.5	1.8	0	2.5	2.8	2.7	1.9
1.6	1.2	0	0	0.8	1.7	1.3	0	0	0.9

Figure 13. Maximum horizontal displacement of all the history points within the model at different time steps; each cell represent a history point within the model and the value in the cell illustrates the maximum horizontal displacement (m) for the specified time step.
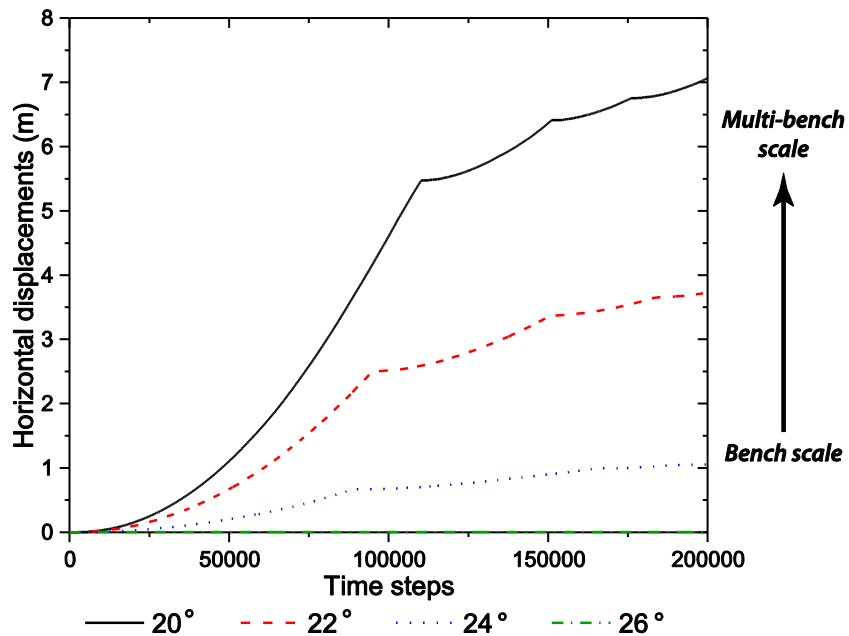

Figure 14. Recorded horizontal displacements for the models presented in Figure 12, with assumed friction angle for the basal surface (Floors)
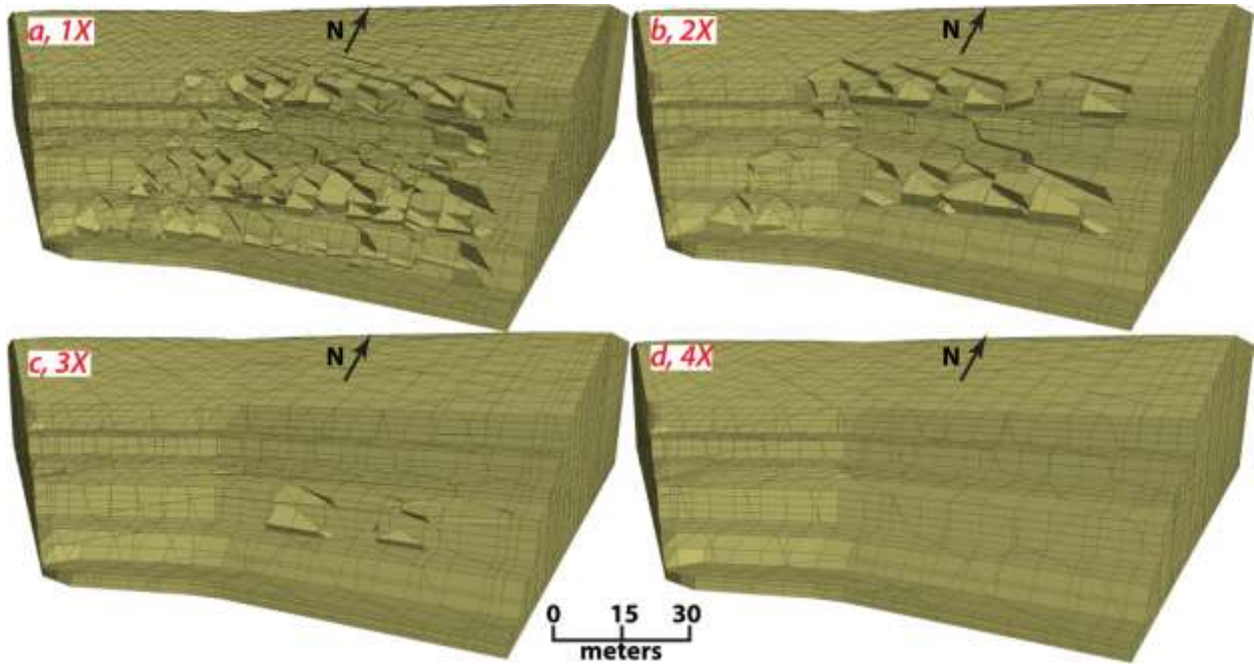
Figure 15. The effect of change in the assumed discontinuity set spacing on the simulated 3DEC failure mechanism; a. initial base model spacing, b. 2X, c. 3X and d. 4X spacing multipliers
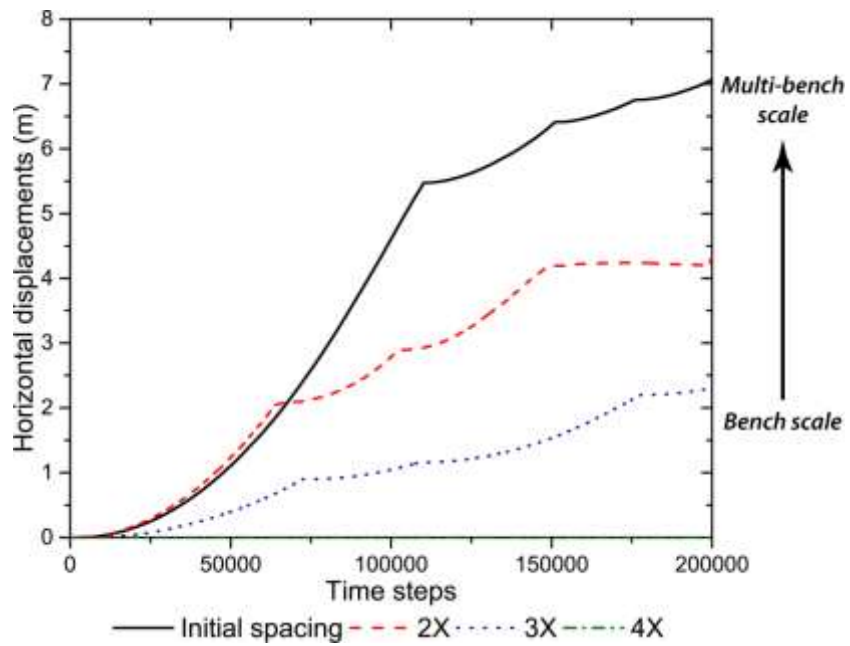

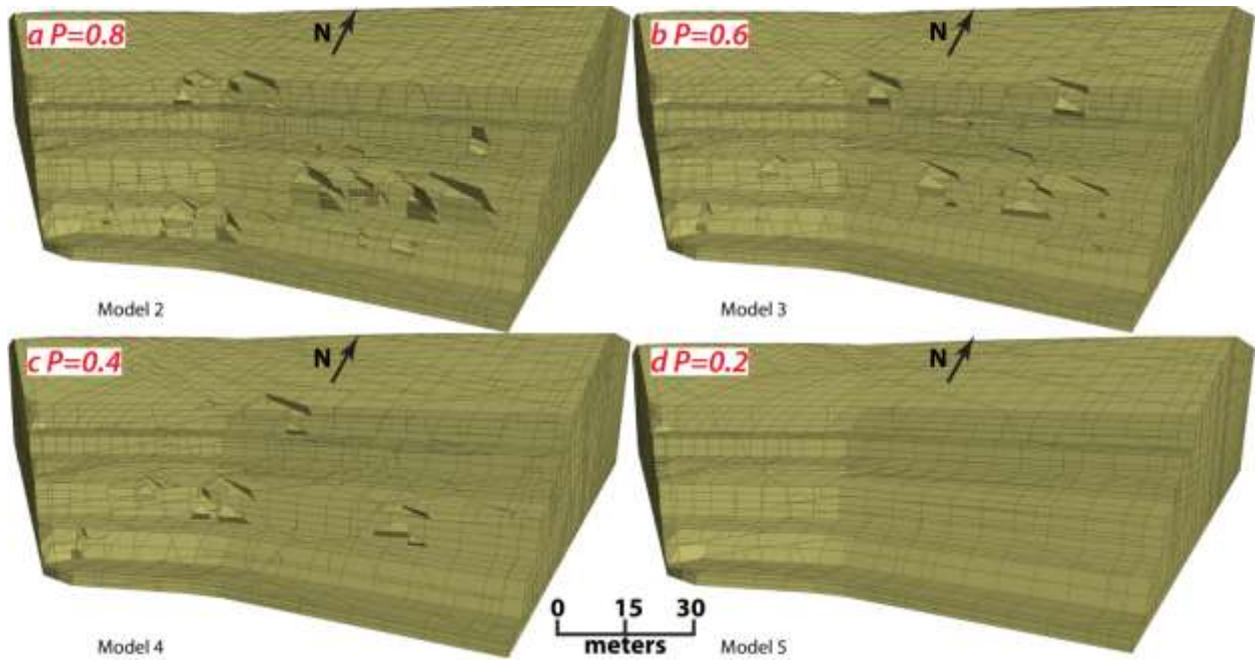**Figure 16. Recorded horizontal displacements for the models presented in Table 6Table 6, with varied joint spacing**

Figure 17. The effect of change in the persistence of the three joint sets on the modelled failure mechanism; a. p = 0.8, b. p = 0.6, c. p = 0.4 and d. p = 0.2)
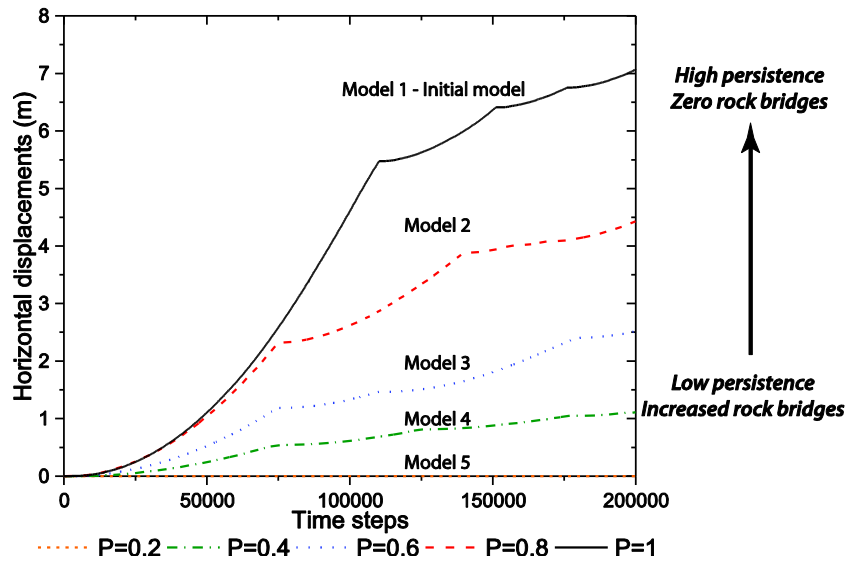

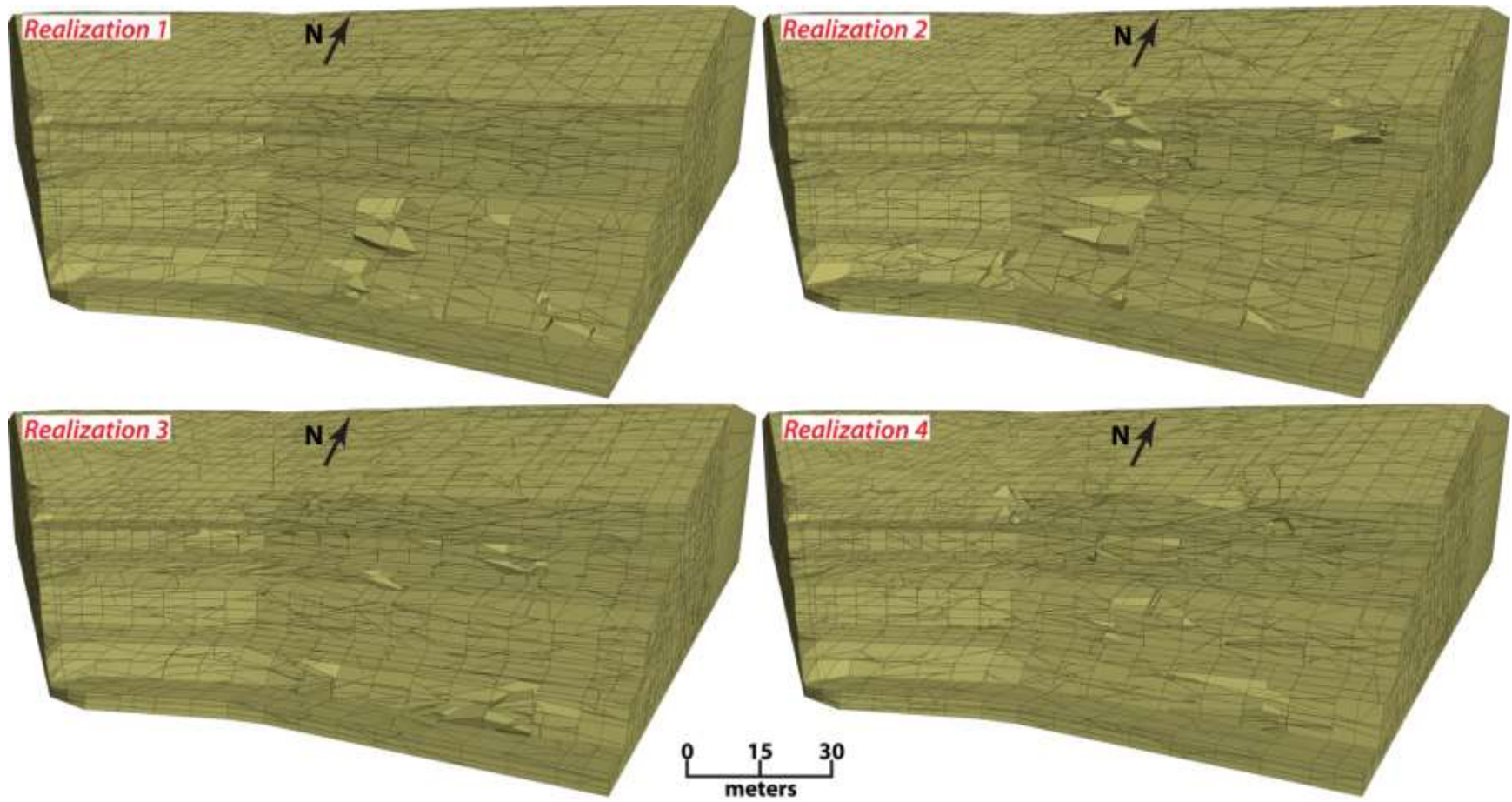**Figure 18. Recorded horizontal displacements for the models with varied persistence values**

Figure 19. Block displacement plots for the four different 3DEC-DFN model realizations

	Deterministic	Stochastic
Block shape	Tetrahedral wedges Pentahedral wedges	Tetrahedral wedges Pentahedral wedges Polyhedral blocks Columnar blocks
Block size	4 to 8 meters	1 to 10 meters

Figure 20. Comparison between block shapes and sizes observed in the deterministic and stochastic models

Realization 1 (120000 steps)					Realization 2 (120000 steps)				
0	0	0	0	0	0	0	0	0	0
0	0	0	0	0	0	0	0	0	0
0	0	0	0	0	0	0	0	2.3	0
0	0	0	0	0	0	0	0	0	0
0	0	0	4.1	0	0	0	2.7	0	0
0	0	0	4.8	0	0	0	0	0	0
Realization 3 (120000 steps)					**Realization 4 (120000 steps)**				
0	0	0	0	0	0	0	0	0	0
0	0	0	0	0	0	0	0	0	0
0	0	0	0	0	0	0	0	5.2	0
0	0	0	0	0	0	0	0.1	0	0
0	0	0	0	0	0	0	0	0	0
0	0	0	2.7	0	0	0	0	0	2.5

Figure 21. Maximum horizontal displacements (m) of all the history points within the DFN models at 120,000 time steps
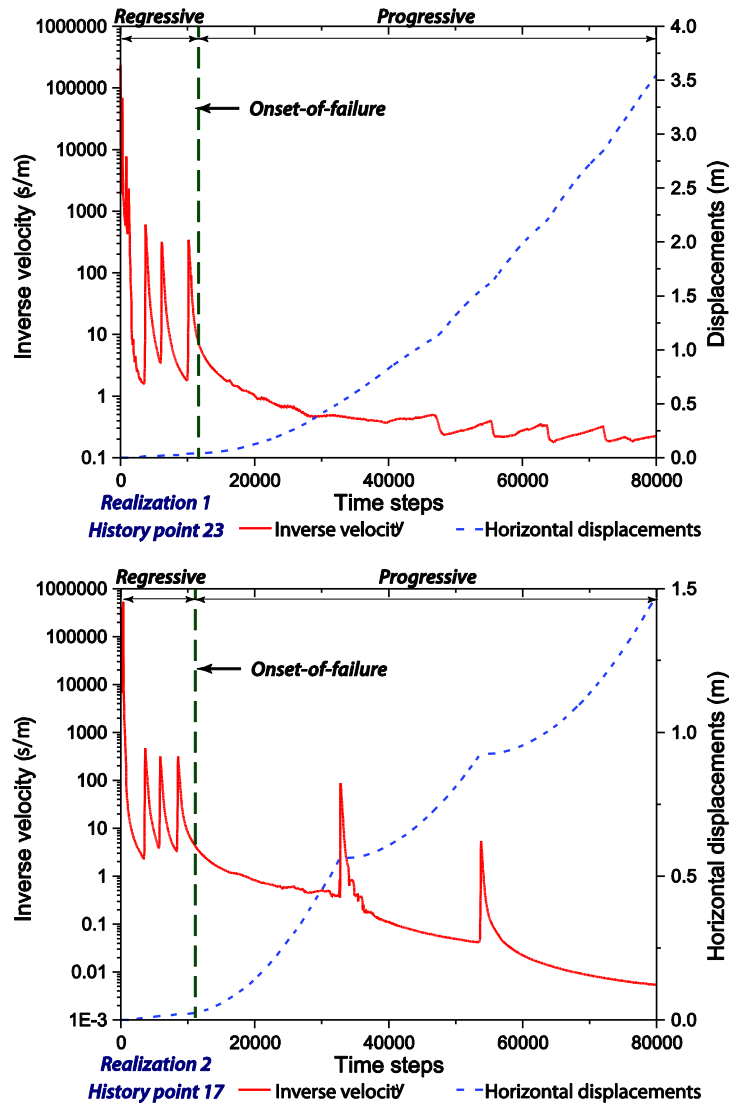
Figure 22. Superimposed plots of inverse velocity, horizontal displacement and onset of slope failure for realization 1 and 2
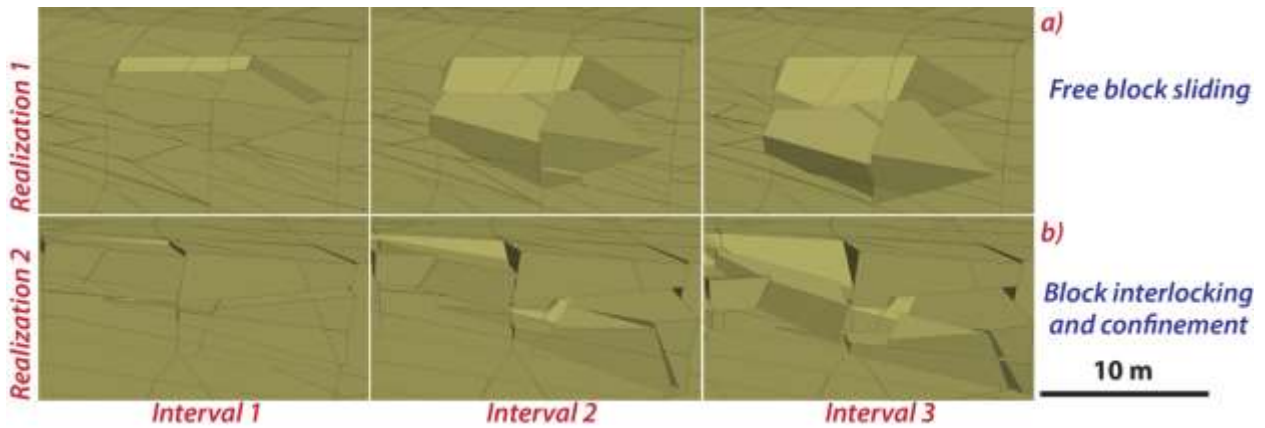

Figure 23. Insets comparing free sliding of the failing blocks in realization 1 with interlocking and confinement of the failing blocks in realization 2